

ULTRA LONG GAMMA-RAY BURSTS FROM THE COLLAPSE OF BLUE SUPER GIANT STARS: AN END-TO-END SIMULATION

ROSALBA PERNA

Department of Physics and Astronomy, Stony Brook University, Stony Brook, NY, 11794, USA

DAVIDE LAZZATI

Department of Physics, Oregon State University, 301 Weniger Hall, Corvallis, OR 97331, USA

MATTEO CANTIELLO

Center for Computational Astrophysics, Flatiron Institute, 162 5th Avenue, New York, NY 10010, USA and
Department of Astrophysical Sciences, Princeton University, Princeton, NJ 08544, USA

Draft version April 19, 2018

ABSTRACT

Ultra-long gamma ray bursts (ULGRBs) are a distinct class of GRBs characterized by durations of several thousands of seconds, about two orders of magnitude longer than those of standard long GRBs (LGRBs). The driving engine of these events has not been uncovered yet, and ideas range from magnetars, to tidal disruption events, to extended massive stars, such as blue super giants (BSG). BSGs, a possible endpoint of stellar evolution, are attractive for the relatively long free-fall times of their envelopes, allowing accretion to power a long-lasting central engine. At the same time, their large radial extension poses a challenge to the emergence of a jet. Here we perform an end-to-end simulation aimed at assessing the viability of BSGs as ULGRB progenitors. The evolution to core collapse of a BSG star model is calculated with the MESA code. We then compute the accretion rate for the fraction of envelope material with enough angular momentum to circularize and form an accretion disk, and input the corresponding power into a jet which we evolve through the star envelope with the FLASH code. Our simulation shows that the jet can emerge, and the resulting light curves resemble those observed in ULGRBs, with durations T_{90} ranging from ≈ 4000 s to $\approx 10^4$ s depending on the viewing angle.

Subject headings: gamma rays: bursts — accretion — black hole physics — stars: massive

1. INTRODUCTION

The class of long Gamma-Ray Bursts (LGRBs), lasting longer than about 2 seconds and with average duration of several tens of seconds, has been unambiguously associated with the core collapse of massive stars. In particular, the direct association of some LGRBs with Type Ic supernovae (SNe; Stanek et al. 2003; Hjorth et al. 2003), implies that these LGRBs are connected to the death of Wolf-Rayet (WR) stars. By the time of the iron core collapse, these stars have lost their hydrogen-rich envelopes, and hence they are significantly more compact than common Type II supernova progenitors. In the standard collapsar scenario (MacFadyen & Woosley 1999), as the core collapses into a black hole (BH), material from the outer layers rains back and forms an accretion disk, if endowed with enough angular momentum to circularize outside of the last stable orbit. Rapid accretion of this disk onto the BH powers a powerful engine. This energy, tapped either via neutrinos (Quian & Woosley 1996; Popham, Woosley & Fryer 1999; Kohri & Mineshige 2002; Lee, Ramirez-Ruiz & Page 2005) or the Blandford-Znajek effect (Blandford & Znajek 1977; see also De Villiers, Hawley & Krolik 2003; Tchekhovskoy, Narayan & McKinney 2011), launches a relativistic jet, which has to punch out of the thick envelope before being able to dissipate and produce gamma-rays. The small size of a WR star facilitates the emergence of the jet (e.g. Matzner 2003). This, combined with the fact that the free-fall time from the outer layers of these stars is several tens of seconds, provides a further theoretical support to the association between long GRBs and WR stars.

In the last several years, a number of GRB events with considerable longer duration has been detected. These bursts, named Ultra Long GRBs (ULGRBs), are characterized by a gamma-ray emission that lasts for several thousands of seconds. When considering the γ -ray component alone, their duration makes them statistically distinct from traditional LGRBs (Boer et al. 2015; Levan 2015). However, if one measures the burst duration also including the X-ray component, which displays plateaus and flares over timescales of several thousands of seconds in many LGRBs, then the evidence for a separate GRB class becomes less clear (Zhang et al. 2014). Theoretically, plateaus and flares have been explained with a variety of models, including magnetars (Rowlinson et al. 2014) and specific progenitor envelope structures for plateaus (Kumar, Narayan & Johnson 2008), and properties of the accretion disk for flares (Perna, Armitage & Zhang 2006; Proga & Zhang 2006). In the case of the ULGRBs, the models which have been proposed essentially fall within three classes: tidal disruption (TD) of a white dwarf (WD) by a black hole (Gendre et al. 2013; Levan et al. 2014; MacLeod et al. 2014; Ioka, Hotokezaka & Piran 2016); a newly born magnetar (Greiner et al. 2015; Gompertz & Fruchter 2017); or fallback accretion from the envelope of an extended progenitor star, such as a blue supergiant (BSG; Quataert & Kasen 2012; Wu et al. 2013; Nakauchi et al 2013; Liu et al. 2018). For the latter scenario, Suwa & Ioka (2011) have suggested that jet breakout is possible in supergiant stars if the envelope accretion and resulting central engine are sufficiently long-lived. Simulations by Nagakura et al. (2012) support this scenario, at least for some moderately extended stellar envelopes

from Pop III massive stars. However, these calculations assumed that all the accreted mass powers a jet, without considering whether the accreting gas in the pre-SN envelope has enough angular momentum to circularize and form a disk.

Generally speaking, for a successful accretion-powered GRB from a massive star, the star at core collapse has to possess material with specific angular momentum larger than the minimum required to circularize at the innermost stable orbit (Woosley 1993; Yoon & Langer 2005; Yoon et al. 2006; Woosley & Heger 2006). The location of this material within the star sets its free-fall time, and ultimately influences the duration of the LGRB, if the jet is able to emerge from the envelope.

In this paper we assess whether the required conditions described above can be realized during the collapse of a massive, radially extended progenitor star. This is achieved via an end-to-end simulation of a relativistic jet propagating through a BSG progenitor. We begin by simulating the evolution and collapse of a massive, rotating BSG star with the MESA code (Paxton et al. 2011; §2), and numerically compute the fallback rate of the rotating, collapsing envelope by following the particle trajectories (§3). The fraction of fallback mass which has enough angular momentum to circularize in an accretion disk provides the power to launch a jet. We simulate the jet evolution through the stellar envelope with the code FLASH (Fryxell et al. 2000), and compute the resulting light curves as a function of the viewing angle with respect to the jet axis (§4). Our results, which are discussed in §5, show that ULGRBs can indeed be produced via this scenario.

2. STELLAR MODEL

In stellar evolution calculations, models for supergiant stars are often found either on a red or a blue solution. Intermediate solutions are thermally unstable (Woosley, Heger & Weaver 2002). In the presence of extreme mass loss, degree of mixing or binary interactions, some massive star calculations can also move towards very high temperatures, ending their evolution as compact WR models. The dichotomy between the LGRB and ULGRB duration can then be interpreted as resulting from the different activity timescale of a central engine that is fed by stellar progenitor envelopes of different radial extension (see Fig. 1). Note that for the core collapse of a Red Super Giant (RSG) progenitor, where envelope material can accrete onto a central black hole due to some fallback or because the SN explosion failed, the extreme size of the envelope imposes a very long ($\sim 10^5$ - 10^6 s) accretion timescale. Therefore, even if the material has enough angular momentum to circularize around the newly formed central object, this can only result in a very small accretion rate. Such accretion rate may not be able to power a jet with enough luminosity to burrow through the prodigious envelope of a RSG, though only dedicated end-to-end simulations can give a definite answer.

For single massive star models, the location on the Hertzsprung-Russell Diagram (HRD) at the end of their evolution depends sensitively on the treatment of mass loss, envelope convection, semiconvection, overshooting and rotational mixing (e.g. Woosley, Heger & Weaver 2002; Maeder & Meynet 2012; Langer 2012; Jiang et al. 2015). The physics of these processes is not fully understood, and their 1D implementations should be considered highly uncertain (e.g. Smith 2013; Cantiello et al. 2014; Jiang et al. 2015). To complicate the picture, the majority of massive stars is found in binary or multiple systems (Sana et al. 2012), with a large fraction of massive stars interacting with one companion dur-

ing their lifetime (De Mink et al. 2014). By changing the size, composition and rotational properties of the stellar envelope, binary interactions can drastically affect the position of a star in the HRD (Langer 2012). In this paper we consider a rapidly-rotating, low-metallicity, single massive star model that ends its life as a blue supergiant with properties that make it attractive as a possible ULGRB progenitor. Given the aforementioned uncertainties, we make no claim that our particular choices of physics should be preferred and/or that this evolutionary channel is the most likely to produce ULGRBs. We just show one possible realization of such evolutionary pathway.

We use Modules for Experiments in Stellar Evolution (MESA, Paxton et al. 2011, 2013, 2015, 2018; release 9793) to create a BSG progenitor model. In our calculations the convective boundaries are determined using the Ledoux criterion and convection is included in the mixing length (MLT) approximation with $\alpha_{\text{MLT}} = 1.82$. We adopt semiconvection with an efficiency $\alpha_{\text{sc}} = 0.1$ (Langer et al. 1983, 1985). The effect of stellar winds is included according to the mass loss scheme described in Glebbeek et al. (2009; Dutch wind scheme) with an efficiency parameter $\eta_{\text{wind}} = 0.8$. We include the physics of internal angular momentum transport accounting for shear instabilities, Eddington-Sweet circulation and magnetic torques. We also account for rotationally enhanced mass loss (Paxton et al. 2013, Perna et al. 2014). Models are evolved from the zero age main sequence to iron core formation.

Our BSG candidate has initial mass $M_{\text{ini}} = 30M_{\odot}$ and metallicity $Z=10^{-5}$, corresponding to $1/1400 Z_{\odot}$. The calculation starts on the zero age main sequence with 55% of Keplerian velocity, corresponding to an equatorial surface velocity of 530 km s^{-1} . Mostly due to the efficient chemical mixing associated with the Eddington-Sweet circulation in rapidly rotating, massive stars (Maeder 1987, Yoon & Langer 2005, Woosley & Heger 2006), the star evolves almost fully mixed during the main sequence. However, unlike the more massive ($M_{\text{ini}} = 40M_{\odot}$) and rapidly rotating model in Fig. 1, which stays quasi-chemically homogenous well after its main sequence becoming a compact WR star, this model manages to develop a larger compositional gradient in its envelope. This compositional gradient allows the model to evolve past its main sequence maintaining a mild core-envelope structure. The large degree of main sequence mixing, however, results in a stellar envelope that is very helium rich. Due to the resulting high mean molecular weight in the envelope, and the reduced line-driven winds at such low-metallicities, the stellar model ends its life as a blue supergiant and with a large amount of angular momentum in its He-rich envelope. The WR and RSG progenitors shown for reference in Fig. 1 were calculated with the same physics prescriptions as for the BSG model, but different values of initial parameters. The bifurcation in the HRD corresponding to rapidly rotating tracks with slightly different values of initial rotation (our BSG and WR models) has been discussed in the literature (see e.g. Maeder 1987), and is due to the sensitivity of rotational mixing to the development of compositional gradients.

A comparison between estimates of the free-fall timescale as a function of the enclosed mass (see e.g. Woosley & Heger 2012),

$$t_{\text{ff}} = \frac{1}{\sqrt{24\pi G \bar{\rho}}}, \quad (1)$$

clearly shows the difference between a WR, a BSG and a RSG

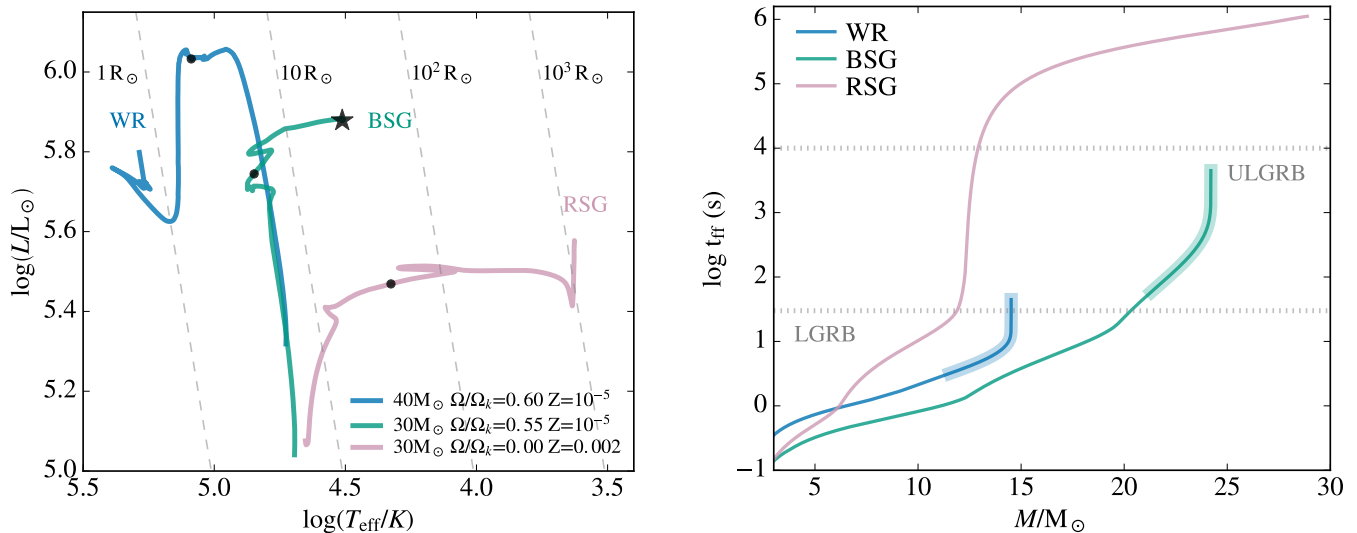


FIG. 1.— *Left:* HR-Diagram showing the evolution of three massive stars from the zero age main sequence to core collapse, calculated with MESA. A non-rotating massive star with $M_{\text{ini}} = 30 M_\odot$ and metallicity $Z=0.002$ evolves as an RSG and is characterized by a large stellar radius. This is a Type II SN progenitor model. A star with $M_{\text{ini}} = 40 M_\odot$, $Z=10^{-5}$ and initial rotation rate $\Omega/\Omega_k = 0.6$ evolves chemically homogeneously as a result of rotational mixing. It stays compact and becomes a WR. In the literature, similar models are discussed as possible progenitors of LGRBs. Our BSG progenitor star has $M_{\text{ini}} = 30 M_\odot$, $Z=10^{-5}$ and initial rotation rate $\Omega/\Omega_k = 0.55$. Unlike our WR star, it does not evolve fully chemically homogeneously, although its envelope experiences a large degree of mixing. This keeps the star blue while preserving an envelope of a few tens R_\odot . The star symbol shows the location of the BSG model used as input for the calculations described in Sec. 3 and Sec. 4. Lines of constant radii (dashed lines) are added for reference. The dot symbols show the location where He burning starts contributing substantially (90% of the stellar luminosity). *Right:* Free-fall timescale as function of mass coordinate for the three models shown in the left panel. The free-fall timescale calculation is approximate, but shows how the BSG model accretion timescale is compatible with ULGRB durations, while for the WR model it is consistent with LGRB durations (see horizontal dotted lines). The highlighted part of the curves shows material for which the specific angular momentum is larger than the specific angular momentum of the last stable orbit around a maximally spinning black hole, and is therefore expected to form an accretion disk.

star (cfr. right panel of Fig. 1). In the equation above, $\bar{\rho}$ is the average enclosed stellar density for a given stellar model at core collapse. In the figure we highlight regions of the stellar models (thicker line) corresponding to material with enough angular momentum to circularize in a disk outside of the last stable orbit of a black hole (assumed maximally spinning here). These regions can power a central engine, and their estimated free-fall timescales can help determining what type of energetic transients they might produce. The difference between the typical timescale of tens of seconds of a WR star, and the tens of thousands of seconds of a BSG star, is clearly evident. For the non-rotating RSG model no regions can circularize, and no central engine is expected to operate.

3. ACCRETION RATE AND JET LUMINOSITY

The calculation of the rate \dot{m}_{fb} with which matter from the collapsing envelope falls back and lands on the equatorial plane is performed using the formalism by Kumar et al. (2008). At $t = 0$, the gas is distributed according to its core-collapse profile, with a velocity field entirely in the $\hat{\phi}$ direction. As the star explodes, the fate of the envelope is sensitively dependent on the explosion energy. For energies $\lesssim 10^{51}$ ergs, and stars up to $\sim 40M_\odot$, the entire envelope falls back (Perna et al. 2014). For simplicity here, we assume that subsequent to the star explosion particles follow a free-fall trajectory, which depends on their initial angular velocity $\Omega(r, \theta)$ and location (r, θ, ϕ) in the pre-SN profile. This assumption implies that we are neglecting pressure forces and any modification to the dynamics due to the SN explosion. By neglecting these effects, the results of our calculations lead to the most conservative estimate for the duration of activity of

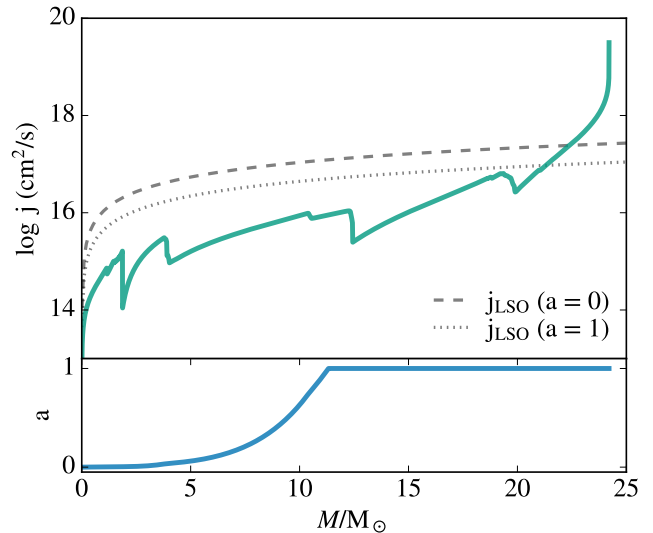


FIG. 2.— *Upper panel:* The angular momentum distribution at core collapse for the BSG star model considered here. The dotted and dashed lines show the specific angular momentum distribution of a particle corotating a BH at the last stable orbit. The dashed line is for the case of a BH with zero spin, while the dotted line for a BH with maximum spin $a = 1$. The mass of the BH is equal to the enclosed mass. *Bottom panel:* BH spin parameter as a function of enclosed mass.

the engine (shortest fallback timescales).

The trajectory of a particle initially positioned at the location (r, θ, ϕ) with angular velocity Ω is characterized by ec-

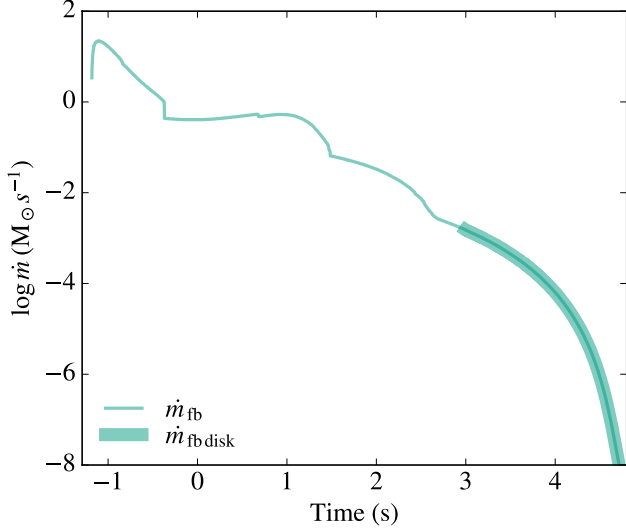


FIG. 3.— Fallback mass rate \dot{m}_{fb} of our BSG model as function of time after core collapse. The highlighted portion of the curve shows the component $\dot{m}_{\text{fb,disk}}$ having enough specific angular momentum to circularize in a disk.

centricity e , given by the expression

$$e = 1 - \frac{\Omega^2}{\Omega_K^2} \sin^2 \theta, \quad (2)$$

where $\Omega_K = (GM_r/r^3)^{1/2}$ is the Keplerian angular velocity of a particle at location r enclosing a mass M_r . The particle reaches the equatorial plane after a time (Kumar et al. 2008)

$$t_{\text{eq}}(r, \theta) = \Omega_K^{-1} [\cos^{-1}(-e) + e(1 - e^2)^{1/2}] (1 + e)^{-3/2} + t_s(r), \quad (3)$$

where the timescale $t_s(r) \approx \Omega_K^{-1}$ corresponds to the sound travel time from the center to the position r . Within the context of Eq. (3), it can be interpreted as the time it takes for information on the loss of pressure after collapse to propagate to position r , after which gas from that location can begin to collapse.

The amount of envelope mass that falls back on the equatorial plane between time t and $t + dt$ is given by

$$dM = \dot{m}_{\text{fb}}(t) dt = 2\pi \int_{r(t)}^{r(t+dt)} dr r^2 \quad (4)$$

$$\times \int_{\theta(t)}^{\theta(t+dt)} d\theta \sin \theta \rho(r, \theta) \delta[t - t_{\text{eq}}(r, \theta)]. \quad (5)$$

Once particles reach the equatorial plane, they can circularize only if their specific angular momentum is equal to or larger than

$$j(R) = \frac{\sqrt{GMR} \left[R^2 - 2(a/c) \sqrt{GMR/c^2} + (a/c)^2 \right]}{R \left[R^2 - 3GMR/c^2 + 2(a/c) \sqrt{GMR/c^2} \right]^{1/2}} \quad (6)$$

at the last stable orbit, where j represents the specific angular momentum of a particle on a co-rotating orbit of a black hole of mass M and angular momentum $J = aM$. Here the coordinate R describes the radial distance in the disk plane.

For the specific case that we are studying here, the angular momentum distribution of the pre-SN profile is shown in

Fig. 2. As a reference, we also display the specific angular momentum distribution of a particle corotating a BH at the last stable orbit for both a non-rotating and a maximally-rotating BH. Inspection of the pre-SN profile shows that only the outermost layers of the envelope have sufficient angular momentum to circularize. Hence, while computing the rate of fallback mass onto the equatorial plane, we further track the component $\dot{m}_{\text{fb,disk}}$ of this rate that has sufficient angular momentum to form a disk. This is the relevant quantity for our simulations. We display $\dot{m}_{\text{fb,disk}}$ in Fig. 3, together with the total fallback accretion rate \dot{m}_{fb} . It is evident that the onset of an accretion-powered engine only happens at ~ 800 – 900 s after the explosion.

Given a certain $\dot{m}_{\text{fb,disk}}$, the fraction of matter which accretes onto the BH is likely not a fixed fraction of $\dot{m}_{\text{fb,disk}}$. At high accretion rates and small radii, cooling is dominated by neutrino emission, and the flow can be described by a neutrino-dominated accretion model, or NDAF (Popham et al. 1999; Di Matteo et al. 2002; Kohri & Mineshige 2002; Janiuk et al. 2004, 2007; Lee et al. 2004, 2005; Kohri et al. 2005). Under these conditions all the matter accretes onto the BH, and hence we can assume $\dot{m}_{\text{acc}} = \dot{m}_{\text{fb,disk}}$. Note that this condition also relies on the fact that the viscous timescale of the disk is much shorter than the fallback timescale, and hence matter flows through the disk at virtually the same rate at which it falls back onto the disk and replenishes it. However, while the condition $\dot{m}_{\text{acc}} = \dot{m}_{\text{fb,disk}}$ safely holds in the NDAF regime, at lower accretion rates, the flow is expected to switch to an advection-dominated accretion flow (ADAF, Narayan & Yi 1994; 1995), with only a fraction of the gas reaching the BH, and with some mass lost to winds (Stone et al. 1999). Given the uncertainties associated with the transition from NDAFs to ADAFs, and the lack of a specific functional form for the amount of mass lost to winds as a function of radius, in the following we will assume that the condition $\dot{m}_{\text{acc}} = \dot{m}_{\text{fb,disk}}$ always holds (where by \dot{m}_{acc} we hence intend the mass that reaches the BH).

Another point to note, which was made by Chen & Beloborodov (2007), is that, during the NDAF phase of the accretion disk, an outflow is likely to be launched only above a critical ‘ignition’ accretion rate, $\dot{M}_{\text{ign}} = K_{\text{ign}} (\alpha_{\text{SS}}/0.1)^{5/3}$ (where α_{SS} is the viscosity parameter, Shakura & Sunyaev 1977), above which the neutrino flux rises dramatically. The value of the constant K_{ign} was found to vary between $0.071 M_{\odot}$ for a spin parameter $a = 0$, and $0.021 M_{\odot}$ for $a = 0.95$ (Chen & Beloborodov 2007). Inspection of Fig. 3 shows that, for our BSG star, such high rates are achieved during a time at which the material that falls back has not enough angular momentum to circularize. The accretion rates which are expected to power the jet are lower than \dot{M}_{ign} . Hence an implication of our model is that the jet-launch mechanism must be of magnetic origin (Blandford & Znajek 1977; De Villiers et al. 2003; Tchekhovskoy et al. 2011). MHD jets from collapsing stars are expected to be stable to kink instabilities (Margalit et al. 2017).

Finally, the jet luminosity can be written as

$$L_{\text{jet}} = \eta \dot{m}_{\text{acc}} c^2, \quad (7)$$

where η is an efficiency factor which parametrizes the fraction of mass converted into energy to power the jet. General-relativistic magneto-hydrodynamic simulations of accretion disks show that the efficiency in converting torus mass and BH spin into jet energy varies between a few percent up to

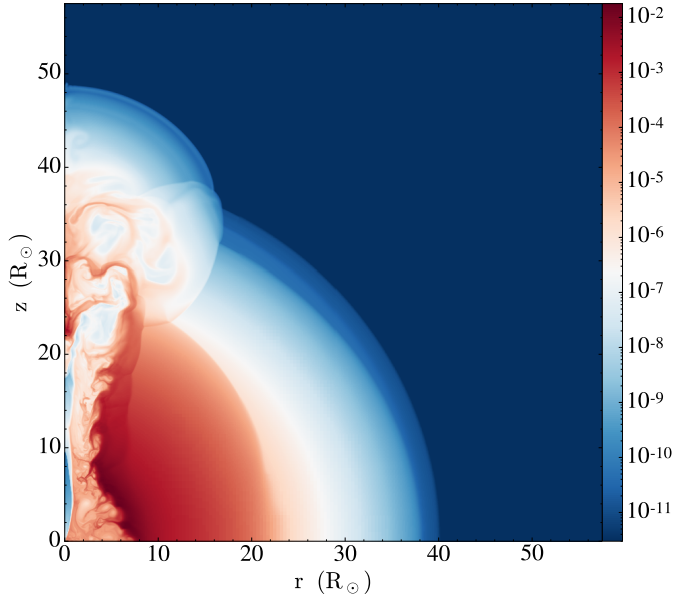


FIG. 4.— Snapshot showing the density structure 400 s after jet launch in our FLASH simulation. The jet breaking out of the BSG envelope structure is clearly visible.

$\approx 100\%$ for maximally spinning BHs (De Villiers et al. 2005; Tchekhovskoy et al. 2011; McKinney et al. 2012; Fragile et al. 2012). The efficiency depends sensitively on the BH spin, the disk thickness, and the magnetic flux. Here we adopt a low value $\eta = 0.01$. Since the ability of the jet to bore through the stellar envelope depends sensitively on its luminosity, our assumption is very conservative. Larger values would result in more powerful jets.

Before continuing with the discussion of the jet propagation within the pre-collapse envelope, we need to emphasize that, since our simulations do not treat the actual SN explosion, we assume that the envelope in which the jet propagates remains fixed to its pre-SN distribution. In reality, as the star explodes and the jet activity pushes material along the jet axis, the mass distribution will change. This effect was discussed by Gilkis, Soker & Papish (2016) in the context of super-energetic SNe (see also Lindner et al. 2010 in the collapsar scenario), but it would similarly apply to our ULGRB scenario. They found that material previously in hydrostatic equilibrium will start moving outward due to the reduced gravity, further extending the duration of the accretion phase.

4. JET EVOLUTION AND GRB LUMINOSITY

The simulation of jet propagation in the pre-SN envelope is performed with the adaptive mesh refinement relativistic hydrodynamic (AMR- RHD) code FLASH (Fryxell et al. 2000), as modified in Morsony et al. (2007; see Figure 4 for a pseudocolor rendering of the density at $t = 400$ s after the jet launch). The jet starts at $t_0 = 989$ s as a boundary condition with time-dependent luminosity given by Eq. (7), where the accretion rate is provided by the fallback mass component able to circularize in a disk prior to accreting ($\dot{m}_{\text{fb,disk}}$; cfr. highlighted curve in Fig. 3). At earlier times, the accreted mass falls directly into the BH and a jet is not launched. The jet is injected with an opening angle $\theta_j = 16^\circ$, compatible with the range of values inferred via different analyses for GRB 111209A ($\theta_j \approx 9^\circ - 11^\circ$, Kann et al. 2017, and $\theta_j = 23^\circ$ Stratta et al. 2013) and the constraint for GRB 121027A

($\theta_j > 10^\circ$; Levan et al. 2014). It should be noted, however, that the injection opening angle can be very different from the opening angle of the cone within which the outflow propagates after breakout off the stellar envelope (e.g., Morsony et al. 2007; see also the discussion below). The jet is injected with an initial Lorentz factor $\Gamma_0 = 5$, and with internal energy that enables acceleration to an asymptotic Lorentz factor $\Gamma = 300$, values that are commonly adopted in long GRB simulations (e.g., Morsony et al. 2007). The computational grid extends in the radial direction from $r_0 = 10^{10}$ cm to $r_{\text{max}} = 4 \times 10^{12}$ cm. The maximum resolution, at the base of the jet, is $\sim 5 \times 10^7$ cm. A polytropic equation of state with adiabatic index $\hat{\gamma} = 4/3$ is adopted throughout the domain. The numerical simulation was run for 1803 seconds, after which the jet-star interaction wanes and the jet luminosity becomes a constant fraction of the luminosity injected at the base.

The light curves as a function of the viewing angle are computed following Morsony et al. (2010) by assuming that a constant fraction of the kinetic luminosity carried by the jet is radiated:

$$L(t) = c\epsilon \int_{\Sigma_R} [(4p + \rho c^2)\Gamma^2 - \rho c^2\Gamma] \delta^2 d\sigma, \quad (8)$$

where ϵ is the radiative efficiency, Σ_R is a spherical surface of radius R centered on the GRB engine, p and ρ are the pressure and comoving density of the jet, respectively, and $\delta = [\Gamma(1 - \beta \cos \theta)]^{-1}$ is the Doppler factor. We calculate the light curves at a radius $R = 3 \times 10^{12}$ cm, when the jet has left the stellar surface, and at a safe distance from the outer boundary of the simulation domain. We assume a radiative efficiency $\epsilon = 0.5$ (Zhang et al. 2007; see also discussion on efficiencies in Giacomazzo et al. 2013), and consider only emission from material moving with a Lorentz factor $\Gamma \geq 10$. Material with lower Lorentz factor does not substantially contribute to the radiated luminosity.

Fig. 5 shows the isotropic equivalent bolometric light curves for a range of viewing angles. Luminosities of the order of 10^{51} erg/s are seen for observers lying within a few tens of degrees from the jet axis. The bright part of the light curve lasts for approximately 1000 s, followed by a smooth decline that tracks the decay of the engine luminosity. We compute the observed duration of our predicted bursts (T_{90}) by integrating the light curves and finding the times at which 5% and 95% of the fluence has been radiated. We stop our numerical simulation at 1803 seconds, since the light curve is well represented by a re-scaled version of the input luminosity at longer times. The resulting duration (T_{90}) is of the order of 10^4 s, in good agreement with observed ULGRBs (see Figure 6). At large viewing angles the duration is shorter. Qualitatively, one can understand this behavior in the following way. As the jet propagates through the stellar progenitor it produces a cocoon (Ramirez-Ruiz et al. 2002; Lazzati & Begelman 2005) that recollimates the jet into an angle that is narrower than the injection value $\theta_j = 16^\circ$. When the jet breaks out of the stellar envelope, the outflow is composed of a fast core of a few degrees opening angle surrounded by slower wings extending to large angles $\theta \sim 45^\circ$. The wings are due to the shearing of the jet sides on the cocoon material and to the cocoon material itself that has high pressure and, once released on the stellar surface, is free to accelerate quasi-isotropically. As time progresses, the confining pressure of the stellar material decreases and the jet widens to its injection value.

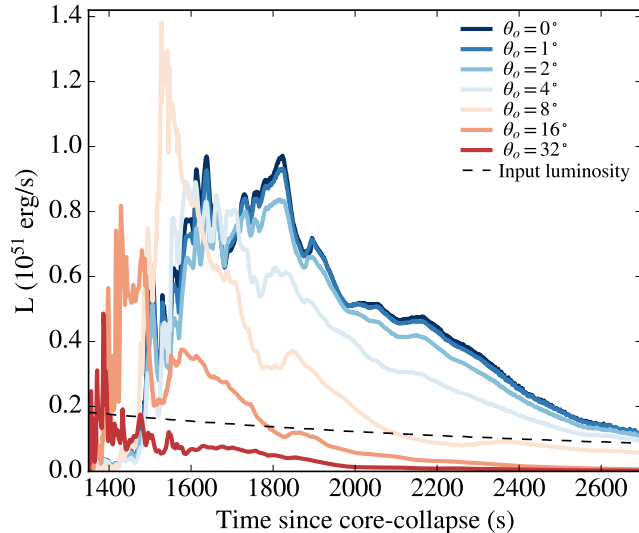


FIG. 5.— Isotropic equivalent bolometric luminosity of the prompt emission, as a function of time from core collapse (the jet is launched at $t = 989$ s in these units and jet breakout occurs around 1389 s), and for a range of viewing angles. At early times, the luminosity is higher than the input one L_{jet} (also shown as isotropic equivalent) since the jet is squeezed by the star pressure into a smaller angle than the one at injection, and because of the sudden release of the cocoon energy, which was trapped within the star up to jet breakout.

As seen in Figure 5, light curves for observers within $\theta_o \lesssim 5^\circ$ are characterized by high luminosity, sustained for at least 1000 s, followed by a decline similar to the luminosity of the central engine. Note that, in the early phase, their isotropic-equivalent luminosity is larger than that of the central engine due to the jet collimation into a narrower opening angle. The observer at the intermediate angle $\theta_o = 8^\circ$ initially receives radiation mainly from the cocoon material. Its light curve rises sharply, analogously to the light curves of observers at wider angles. Note that, despite the fact that the cocoon is less collimated than the jet, its luminosity can instantaneously exceed the input one due to the fact that the cocoon carries energy stored within the star as the jet propagates. This stored energy gets released and converted into radiation after the jet breaks out. The bright phase lasts for about 400 s, after which the luminosity decreases. When the jet opening angle regains the injection value at $t \sim 3000$ s, however, the light curve seen by the $\theta_o = 8^\circ$ observer becomes very similar to the ones of observers with $\theta_o < 5^\circ$. At even wider angles $\theta_o > 16^\circ$, observers only receive emission from the cocoon, and the light curves decrease fairly quickly in a few hundred seconds.

5. DISCUSSION

We have performed an end-to-end simulation of an ULGRB from the collapse of a BSG star. Our stellar progenitor is a particularly low-metallicity, rapidly-rotating massive star model. At core collapse, such model fails to produce a canonical LGRB because of the presence of a relatively extended envelope which sets an accretion timescale much longer than that typical of LGRBs, and at the same time prevents the very inner regions from retaining enough angular momentum to satisfy the collapsar scenario. This model, while staying largely mixed for the duration of its main sequence, does not evolve quasi-chemically homogeneously (Maeder 1987; Yoon & Langer, 2005; Woosley & Heger 2006). It manages to

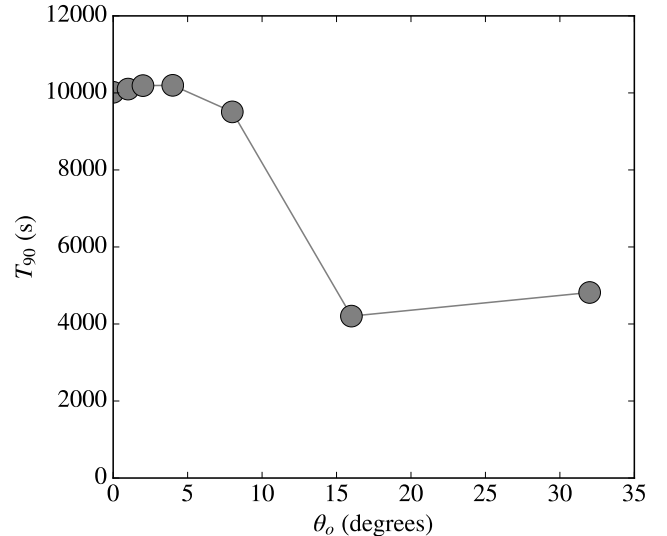


FIG. 6.— T_{90} duration of the bursts from our simulation as a function of the observer angle. Note that the duration becomes shorter at viewing angles larger than the opening angle at injection. See text for a discussion.

build a compositional gradient, which stops further mixing and allows to develop a core-envelope structure. Due to the low-metallicity and the high helium fraction of the envelope, this model only expands to few tens of solar radii (compared to the $\approx 1000 R_\odot$ of typical RSGs), with the outer layers unable to lose too much angular momentum through stellar winds. At core collapse, such BSG model can produce an accretion disk around a newly formed central object with accretion timescale $\approx 10^4$ s. It is important to note that this particular solution exists for a small region of the parameter space of initial rotational velocity. That is, fixing all other parameters, models initialized with slightly different values of initial rotational velocity can end up producing either a WR (mostly for faster rotation) or a RSG (mostly for slower rotation). A precise quantitative prediction of which stars should end up producing BSG through this channel is difficult, since the physics of internal chemical mixing depends on a number of poorly understood processes. The important point is that if LGRBs are produced through quasi-chemically-homogeneous evolution, then this channel has to exist. This is because it operates in models with similar masses and metallicities, but just rotating a bit slower than those producing LGRBs. Therefore, if this channel dominates the production of ULGRBs, these explosions should be found in environments not too dissimilar from those of LGRBs (tracing similar stellar populations). ULGRBs should also have lower rates than LGRBs, since overall they require initial rotation rates in a smaller region of the parameter space. These expected trends are only tentative: more quantitative predictions require calculating grids of massive star models of different mass, metallicity and with fine resolution in the initial rotation rate, to be weighted with appropriate initial functions for the various stellar parameters.

The final properties of our ULGRB model are fairly similar to those of single BSG models studied by Woosley & Heger (2012) in the context of “Type 3 collapsars”, core collapse events for which only the surface layers of the star have enough rotation to form a disk and the SN shock is so weak that these layers are not ejected. Their BSG models were calculated with initial metallicity $Z = 1/10 Z_\odot$ and lower initial rotation rate (about 20% of the Keplerian value), showing that

similar outcomes can be produced for a less restrictive set of initial parameters. In the specific case studied here, the choice of a much lower metallicity and larger rotation rate was dictated by the requirement to produce relatively compact and He-rich BSGs at core collapse (our BSG model is more compact and He-rich than the one of Woosley & Heger 2012, with an envelope having a helium mass fraction larger than 0.7). A large surface helium abundance is suggested by the observations of ULGRB 11209A, for which the underlying superluminous supernova SN 2011kl was found to lack hydrogen lines in the spectra (Greiner et al. 2015; but see also Ioka et al. 2016).

Finally, we remark that the scenario discussed here is not the only possible way of producing rapidly rotating BSGs. These stars can be a result of, e.g., binary stellar evolution and/or different combinations of initial values of rotation, mass, metallicity as well as choices of the physics of internal mixing (see e.g. Woosley & Heger 2012). Because of

this, we do not claim that the particular scenario discussed in the paper should be favored. We just show that it is possible to produce evolutionary calculations of BSGs to core collapse that, as part of an end-to-end calculation, can produce the observed properties of ULGRBs.

RP acknowledges support from the NSF under grant AST-1616157. DL acknowledges support from NASA grant NNX17AK42G. The Flatiron Institute is supported by the Simons Foundation.

SOFTWARE

Python available from python.org, Matplotlib (Hunter 2007), ipython/jupyter (Pérez & Granger 2007, Kluyver et al. 2016), yt (Turk et al. 2011). MESA inlists, data and the source code to produce the figures in this paper are available at <https://github.com/matteocantiello/ulgrb>

REFERENCES

- Blandford, R. D., Znajek, R. L. 1977, *MNRAS*, 179, 433
 Boer, M., Gendre, B., & Stratta, G. 2015, *Astrophys. J.*, 800, 16
 Cantiello, M., Mankovich, C., Bildsten, L., Christensen-Dalsgaard, J., Paxton, B. 2014, *ApJ*, 788, 93
 Chen, W.-X. & Beloborodov, A. 2007, *ApJ*, 657, 383
 de Mink, S. E., Sana, H., Langer, N., Izzard, R. G., Schneider, F. R. N. 2014, *ApJ*, 782, 7
 De Villiers, J.-P., Hawley, J. F., Krolik, J. H. 2003, *ApJ*, 599, 1238
 De Villiers, J.-P., Hawley, J. F., Krolik, J. H., & Hirose, S. 2005, *ApJ*, 620, 878
 Di Matteo, T., Perna, R., & Narayan, R. 2002, *ApJ*, 579, 706
 Fragile, P. C., Wilson, J., & Rodriguez, M. 2012, *MNRAS*, 424, 524
 Fryxell, B., et al. 2000, *ApJS*, 131, 273
 Gendre, B., Stratta, G., Atteia, J. L., et al. 2013, *ApJ*, 766, 30
 Giacomazzo, B., Perna, R., Rezzolla, L., Troja, E., Lazzati, D. 2013, *ApJ*, 762L, 18
 Giannios, D. 2012, *MNRAS*, 422, 3092
 Gilkis, A., Soker, N. & Papish, O. 2016, *ApJ*, 826, 178
 Glebbeek, E., Gaburov, E., de Mink, S. E., Pols, O. R., Portegies Zwart, S. F. 2009, *A&A*, 497, 255
 Gompertz, B., Fruchter, A. 2017, *ApJ*, 839, 49
 Greiner, J., Mazzali, P. A., Kann, D. A., et al. 2015, *Nature*, 523, 189
 Hjorth, J., Sollerman, J., Moller, P., et al. 2003, *Natur*, 423, 847
 Hunter, J. D., 2007, *IEEE Computer Soc.*, 9, 3, 90–95
 Ioka, K., Hotokezaka, K., & Piran, T. 2016, *ApJ*, 833, 110
 Janiuk, A., Perna, R., Di Matteo, T., Czerny, B. 2004, *MNRAS*, 355, 950
 Janiuk, A., Yuan, Y., Perna, R., Di Matteo, T. 2007, *ApJ*, 664, 1011
 Jiang, Y.-F., Cantiello, M., Bildsten, L., Quataert, E. Blaas, O. 2015, *ApJ*, 813, 74
 Kann, D. A. et al. 2017, [arXiv:1706.00601](https://arxiv.org/abs/1706.00601)
 Kluyver, T., Ragan-Kelley, B., Pérez F., et al. 2016, *Proceedings of the 20th ICEP*, IOS Press, 87
 Kohri, K., & Mineshige, S. 2002, *ApJ*, 577, 311
 Kohri, K., Narayan, R., & Piran, T. 2005, *ApJ*, 629, 341
 Kumar, P., Narayan, R., & Johnson, J. L. 2008, *MNRAS*, 388, 1729
 Langer, N. 2012, *ARA&A*, 50, 107
 Langer, N., Fricke, K. J., Sugimoto, D. 1983, *A&A*, 126, 207
 Langer, N., El Eid, M. F., Fricke, K. J. 1985, *A&A*, 145, 179
 Lazzati, D., Begelman, M. C. 2005, *ApJ*, 629, 903
 Lazzati, D., Morsony, B. J., Margutti, R., Begelman, M. C. 2013, *ApJ*, 765, 103
 Lazzati, D. 2016, *ApJ*, 829, 76
 Lazzati, D., Lopez-Camara, D., Cantiello, M., Morsony, B. J., Perna, R., Workman, J. C. 2017, 848L, 6
 Lee W. H., Ramirez-Ruiz E., Page D., 2004, *ApJ*, 608, L5
 Lee W. H., Ramirez-Ruiz E., Page D., 2005, *ApJ*, 632, 421
 Levan, A. J., Tanvir, N. R., Starling, R. L. C., et al. 2014, *ApJ*, 781, 13
 Lindner, C. C., Milosavljevic, M., Couch, S. M. & Kumar, P. 2010, *ApJ*, 713, 800
 Liu, T., Song, C.-Y., Zhang, B., Gu, W.-M. Heger, A. 2018, *ApJ*, 852, 20
 Maeder, A. 1987, *A&A*, 178, 159–169
 Maeder, A., Meynet, G. 2012, *Rev. Mov.Phys.* 84, 25
 MacFadyen, A. I. & Woosley, S. E. 1999, *ApJ*, 524, 262
 MacLeod, M., Goldstein, J., Ramirez-Ruiz, E., Guillochon, J., & Samsing, J. 2014, *ApJ*, 794, 9
 Margalit, B., Metzger, B. D., Thompson, T. A., Nicholl, M., Sukhbold, T. 2017, [arXiv:1705.01103](https://arxiv.org/abs/1705.01103)
 McKinney, J. C., Tchekhovskoy, A., & Blandford, R. D. 2012, *MNRAS*, 423, 3083
 Morsony, B. J., Lazzati, D., Begelman, M. C. 2007, *ApJ*, 665, 569
 Nakauchi, D., Kashiyama, K., Suwa, Y., & Nakamura, T. 2013, *ApJ*, 778, 67
 Nagakura, H., Suwa, Y., Ioka, K. 2012, *ApJ*, 754, 85
 Narayan, R. & Yi, I. 1994, *ApJ*, 428, L13
 Narayan, R. & Yi, I. 1995, *ApJ*, 444, 231
 Paxton, B., et al. 2011, *ApJS*, 192, 3
 Paxton, B., et al. 2013, *ApJS*, 208, 4
 Paxton, B. et al. 2015, *ApJS*, 220, 15
 Paxton, B. et al. 2018, *APJS*, 234, 34
 Pérez F., & Granger, B.E. 2007, *Computing in Science & Engineering*, 9, 21
 Perna, R., Duffell, P., Cantiello, M., MacFadyen, A. I., 2014, *ApJ*, 781, 119
 Perna, R., Armitage, P. J., Zhang, B. 2006, *ApJL*, 636, 29
 Popham, R., Woosley, S. E., & Fryer, C. 1999, *ApJ*, 518, 356
 Proga, D., Zhang, B. 2006, *MNRAS*, 360L, 71
 Quataert, E.; Kasen, D. 2012, *MNRAS*, 419L, 1
 Qian, Y.-Z.; Woosley, S. E. 1996, *ApJ*, 471, 331
 Ramirez-Ruiz, E., Celotti, A., Rees, M. J. 2002, *MNRAS*, 337, 1349
 Rowlinson, A., Gompertz, B. P., Dainotti, M., O’Brien, P. T., Wijers, R. A. M. J., van der Horst, A. J. 2014, *MNRAS*, 443, 1779
 Sana, H. et al. 2012, *Science*, 337, 444
 Shakura, N. I.; Sunyaev, R. A. 1973, *A&A*, 24, 337
 Smith, N. 2013, *MNRAS*, 429, 2366 Research supported by the National Science Foundation. New York, Wiley-Interscience
 Stanek, K. Z., Matheson, T., Garnavich, P. M., et al. 2003, *ApJL*, 591, L17
 Stratta, G., Gendre, B., Atteia, J. L., et al. 2013, *ApJ*, 779, 66
 Suwa, Y., Yoka, K., et al. 2011, *ApJL*, 726, 107
 Tchekhovskoy, A., Narayan, R., McKinney, J. C. 2011, *MNRAS*, 418L, 79
 Turk, M. J., Smith, B. D., Oishi, J. S., et al. 2011, *ApJS*, 192, 9
 Yoon, S.-C., Langer, N. 2005, *A&A*, 443, 643
 Yoon, S.-C., Langer, N., Norman, C. 2006, *A&A*, 460, 199
 Woosley, S. E. 1993, *ApJ*, 405, 273
 Woosley, S. E., Heger, A. 2006, *ApJ*, 637, 914
 Woosley, S. E., Heger, A., Weaver, T. A. 2002, *Rev of Mod. Phys.*, 74, 1015
 Wu, X.-F., Hou, S.-J., Lei, W.-H. 2013, *ApJ*, 767L, 36
 Zhang, B.-B., Zhang, B., Murase, K., Connaughton, V., Briggs, M. 2014, 787, 66
 Zhang, B. et al. 2007, *ApJ*, 655, 989